

RESEARCH ARTICLE

# Visualization of Subunit Interactions and Ternary Complexes of Protein Phosphatase 2A in Mammalian Cells

Shu-Ting Mo<sup>1</sup>, Shang-Ju Chiang<sup>1</sup>, Tai-Yu Lai<sup>2</sup>, Yu-Ling Cheng<sup>1</sup>, Cheng-En Chung<sup>1</sup>, Spencer C. H. Kuo<sup>3</sup>, Kelie M. Reece<sup>5</sup>, Yung-Cheng Chen<sup>1</sup>, Nan-Shan Chang<sup>1,2,4</sup>, Brian E. Wadzinski<sup>5\*</sup>, Chi-Wu Chiang<sup>1,2,4\*</sup>

1. Institute of Molecular Medicine, College of Medicine, National Cheng Kung University, Tainan, Taiwan, 2. Institute of Basic Medical Sciences, College of Medicine, National Cheng Kung University, Tainan, Taiwan, 3. Department of Medicine, College of Medicine, National Cheng Kung University, Tainan, Taiwan, 4. Center for Infectious Disease and Signaling Research, National Cheng Kung University, Tainan, Taiwan, 5. Department of Pharmacology, Vanderbilt University Medical Center, Nashville, TN, United States of America

\*chiangcw@mail.ncku.edu.tw (CWC); brian.wadzinski@vanderbilt.edu (BEW)



CrossMark  
click for updates

OPEN ACCESS

**Citation:** Mo S-T, Chiang S-J, Lai T-Y, Cheng Y-L, Chung C-E, et al. (2014) Visualization of Subunit Interactions and Ternary Complexes of Protein Phosphatase 2A in Mammalian Cells. PLoS ONE 9(12): e116074. doi:10.1371/journal.pone.0116074

**Editor:** Veerle Janssens, Faculty of Medicine, Belgium

**Received:** November 7, 2014

**Accepted:** December 1, 2014

**Published:** December 23, 2014

**Copyright:** © 2014 Mo et al. This is an open-access article distributed under the terms of the [Creative Commons Attribution License](https://creativecommons.org/licenses/by/4.0/), which permits unrestricted use, distribution, and reproduction in any medium, provided the original author and source are credited.

**Data Availability:** The authors confirm that all data underlying the findings are fully available without restriction. All relevant data are within the paper and its Supporting Information files.

**Funding:** This study was supported by the Headquarters of University Advancement, National Cheng Kung University (D100-35B58 to C.W.C.), National Science Council (NSC99-2320-B-006-024-MY3 to C.W.C.) and National Institutes of Health (GM051366 to B.E.W.). The funders had no role in study design, data collection and analysis, decision to publish, or preparation of the manuscript.

**Competing Interests:** The authors have declared that no competing interests exist.

## Abstract

Protein phosphatase 2A (PP2A) is a ubiquitous phospho-serine/threonine phosphatase that controls many diverse cellular functions. The predominant form of PP2A is a heterotrimeric holoenzyme consisting of a scaffolding A subunit, a variable regulatory B subunit, and a catalytic C subunit. The C subunit also associates with other interacting partners, such as  $\alpha 4$ , to form non-canonical PP2A complexes. We report visualization of PP2A complexes in mammalian cells. Bimolecular fluorescence complementation (BiFC) analysis of PP2A subunit interactions demonstrates that the B subunit plays a key role in directing the subcellular localization of PP2A, and confirms that the A subunit functions as a scaffold in recruiting the B and C subunits to form a heterotrimeric holoenzyme. BiFC analysis also reveals that  $\alpha 4$  promotes formation of the AC core dimer. Furthermore, we demonstrate visualization of specific ABC holoenzymes in cells by combining BiFC and fluorescence resonance energy transfer (BiFC-FRET). Our studies not only provide direct imaging data to support previous biochemical observations on PP2A complexes, but also offer a promising approach for studying the spatiotemporal distribution of individual PP2A complexes in cells.

## Introduction

Protein phosphatase 2A (PP2A) is a major phospho-serine/threonine protein phosphatase in eukaryotic cells that regulates a variety of essential cellular events [1]. The mature PP2A holoenzyme consists of a scaffolding A subunit, a variable B regulatory subunit, and a catalytic C subunit (PP2Ac). The 36 kDa C subunit is highly conserved in eukaryotic cells, and current models suggest that prior to forming a mature PP2A holoenzyme, PP2Ac first associates with the 65 kDa A subunit to form the AC core dimer. The core dimer then associates with a third, highly variable regulatory B subunit to form a heterotrimeric holoenzyme (ABC). The diverse B regulatory subunits are thought to control the substrate specificity and subcellular localization of the PP2A holoenzyme. Four distinct B subunit families have been identified, including B (B55 or PR55) [2–4], B' (B56 or PR61) [5,6], B'' (PR72) [7] and B''' (PR93/PR110) [8]. The individual B subunits are differentially expressed in tissues, cells, and located in distinct subcellular compartments [1]. In the B55 subfamily, B55 $\alpha$ , B55 $\beta$ 1, and B55 $\delta$  are primarily cytoplasmic, whereas B $\beta$ 2 is localized to mitochondria [9], and B55 $\gamma$  is enriched in the cytoskeletal fraction [10]. The B56 subfamily members B56 $\alpha$ , B56 $\beta$ , and B56 $\epsilon$  are mainly cytoplasmic, but B56 $\gamma$ 1, B56 $\gamma$ 3 and B56 $\delta$  are concentrated in the nucleus [11]. These observations, together with studies of *Saccharomyces cerevisiae* strains lacking individual B subunit genes [12], provide support for a role of B subunit in directing the subcellular localization of the PP2A holoenzyme.

Besides association with the A and B subunits, the C subunit also forms a complex with other proteins, such as  $\alpha$ 4, which appears to be the mammalian homologue of the yeast Tap42 protein. The target of rapamycin (TOR) kinase regulates Tap42 binding with the yeast protein phosphatase catalytic subunits Pph21/22 and SIT4 [13], which are the yeast homologues of mammalian PP2A and PP6, respectively. In mammalian cells,  $\alpha$ 4 associates with the C subunit in the absence of the A and B subunits [14,15], and participates in a wide array of cellular activities such as apoptosis [16], DNA damage response [17], and cell migration [18]. The cellular functions of  $\alpha$ 4 may be mediated via its ability to stabilize the catalytic subunits of PP2A family members (PP2Ac, PP4c, and PP6c) and prevent their degradation [17,19,20]. The phosphatase stabilizing role of  $\alpha$ 4 is further supported by recent structural studies, which suggest that  $\alpha$ 4 binding to PP2Ac stabilizes an inactive conformation of the phosphatase by local unfolding near the active site and steric hindrance of a ubiquitination site on PP2Ac [21].  $\alpha$ 4 also promotes the conversion of PP2A holoenzymes to  $\alpha$ 4-PP2Ac complexes upon perturbation of the active site [21].

Most of our knowledge regarding PP2A complexes has been based on *in vitro* analyses of individual subunits or isolated complexes. However, the assembly and disassembly of PP2A oligomers may be highly dynamic and subject to regulation by various cellular cues [22]. Thus, the subcellular localization of one PP2A subunit may not necessarily reflect the localization of the respective ABC holoenzyme. Although spatial and temporal changes of some PP2A subunits have been observed using immunohistochemical and fluorescent techniques, direct

visualization of PP2A oligomeric complexes in cells has not been reported until now.

Several approaches have been applied to investigate protein-protein interactions, including bimolecular fluorescence complementation (BiFC) [23] and fluorescence resonance energy transfer (FRET) [24, 25]. BiFC is based on reconstituting a fluorophore by the association of two halves of a fluorescent protein when the fragments are assembled into the same macromolecular complex [23]. FRET occurs when a donor fluorophore is brought into close proximity (less than 10 nm) to an appropriate acceptor fluorophore [24, 25]. Studies of the crystal structures of PP2A complexes [26] prompted us to use BiFC [22] to visualize dimeric PP2A subunit interactions, and combined BiFC and FRET [23–25] to visualize ternary PP2A complexes. Our BiFC analyses not only confirmed that the A subunit functions as a scaffold for the B and C subunits, but also demonstrated that the B subunit directs the localization of PP2A holoenzymes. In addition, our BiFC studies demonstrated that  $\alpha 4$  promotes formation of the PP2A dimeric (AC) core enzyme by stabilizing the C subunit. Moreover, for the first time, we successfully visualized two different PP2A holoenzyme complexes,  $A\alpha/B56\gamma 3/C\alpha$  and  $A\alpha/B55\beta 2/C\alpha$ , in cells by applying BiFC in conjunction with FRET (BiFC-FRET) [27].

## Materials and Methods

### Cell culture, cell lines, and transfection

NIH3T3 cells were cultured in Dulbecco's modified Eagle's medium (DMEM) supplemented with 10% bovine serum (BS). Mammalian expression plasmids were transfected into NIH3T3 cells using Lipofectamine 2000 (Invitrogen) and the manufacturer's recommended protocol. Twenty-four hours after transfection, cells were fixed or harvested for further analysis.

### DNA constructs

The construction of expression plasmids are described in [S1 Text](#). Mammalian expression plasmids for BiFC and primers for the PCR-based cloning strategies are described in [S1](#) and [S2 Tables](#).

### Immunofluorescence and microscopy

Following transfection or indicated treatments, cells were washed three times with PBS, fixed by a solution containing 4% paraformaldehyde and 0.025% glutaraldehyde for 15 min, and permeabilized with 0.1% Triton-X-100 for 30 min. Cells were then blocked with 5% BSA in PBS for 1 h, and subsequently incubated with anti-HA (Cell Signaling, 2367) or anti-Myc tag (Cell Signaling, 2278) antibody for 1 h, followed by incubation with Cy3-conjugated secondary antibodies (Jackson ImmunoResearch). Cells were then stained with 4', 6-diamidino-2-phenylindole dihydrochloride (DAPI) for 5 min, mounted, and

visualized by fluorescence microscopy (Zeiss, Axio observer Z1) and confocal microscopy (Olympus, FV1000). Quantitation of subcellular distribution of immunostained proteins was carried out by both unbiased visual judgment and assessment on fluorescence intensity in both nucleus and cytoplasm using Zeiss AxioVision software.

### Co-immunoprecipitation and Western blotting

Whole cell lysates for Western analysis and immunoprecipitations were prepared in radioimmunoprecipitation assay buffer (RIPA) and isotonic immunoprecipitation buffer, respectively [28]. Immunoprecipitations were performed as previously described [29]. Briefly, whole cell lysates were incubated overnight with anti-HA (HA.11, Covance) or anti-Myc (Cell Signaling, 2278) antibodies, and the immune complexes were precipitated using protein A/G-Sepharose, followed by SDS-PAGE and Western blotting analysis using the following primary antibodies: anti-HA (Cell Signaling, 2367); anti-Myc (Cell Signaling, 2278); anti-Flag M2 (Sigma, F3165); anti- $\beta$  actin (Sigma, A5441); anti-PP2A/A (Santa Cruz, sc-6112); anti-C $\alpha$  (BD Transduction Laboratories, 610556). After incubation with the primary antibodies and corresponding HRP-conjugated secondary antibodies, the blots were developed by enhanced chemiluminescence.

### BiFC analysis

For analysis of interactions between A and B subunits and between A and C subunits, NIH3T3 cells were seeded at a density of  $7 \times 10^4$ /well onto coverslips within 24-well plates and transiently transfected with 1  $\mu$ g total DNA containing equal amounts of BiFC constructs encoding N-terminally or C-terminally YFPN-(YN-) or YFPC-(YC-) fused A $\alpha$ , PP2A $\alpha$ , and the B subunit in various combinations as indicated in the text. For analysis of interactions between B and C subunits, equal amounts of BiFC constructs encoding YN- or YC-fused PP2A $\alpha$  and YC- or YN-fused various B subunits with or without pCA2-6MYC-A $\alpha$  were co-transfected into NIH3T3 cells. For assessing the specificity of BiFC between A and B subunits in the presence of SV40 small t antigen, NIH3T3 cells were transfected with BiFC constructs encoding A $\alpha$ -YC or YC-A $\alpha$ , YN-fused B subunit, and pCMV5-small T<sub>WT</sub>, pCMV5-small T<sub>MUT</sub>, or empty vector (relative amount of YC-A $\alpha$ :YN-B:pCMV5-small T<sub>WT</sub>, -small T<sub>MUT</sub>, or empty vector was 1:1:2). For analysis of A/B complexes in cells synchronized in the early S phase, NIH3T3 cells were transfected with the indicated BiFC constructs and 24 h post-transfection, cells were treated with 10  $\mu$ g/ml aphidicolin for 12 h. For analysis of interactions between PP2Ac and  $\alpha$ 4, equal amounts of BiFC constructs encoding YC-P2A $\alpha$  and YN- $\alpha$ 4<sub>WT</sub> or YN- $\alpha$ 4<sub>MUT</sub> were co-transfected into NIH3T3 cells. For assessing the effect of  $\alpha$ 4 on interactions between A and C subunits, equal amounts of BiFC constructs encoding YN-A $\alpha$  and PP2A $\alpha$ -YC and an empty vector or a vector harboring  $\alpha$ 4<sub>WT</sub>, or  $\alpha$ 4<sub>MUT</sub> were co-transfected into NIH3T3 cells. Twenty-four hours post-transfection, cells were washed, fixed, and visualized by fluorescence

microscopy (Zeiss, Axio observer Z1) at  $200\times$  magnification and confocal microscopy (Olympus, FV1000) at  $600\times$  magnification. Quantitation of subcellular distribution of BiFC signals was carried out by both unbiased visual judgment and assessment on fluorescence intensity in both nucleus and cytoplasm using Zeiss AxioVision software.

### BiFC-FRET analysis

For visualizing PP2A  $A\alpha B56\gamma3C\alpha$  holoenzyme complexes by BiFC-FRET analysis, NIH3T3 cells were transfected with BiFC constructs encoding YC- $A\alpha$  and YN-B56 $\gamma3$  and a construct for PP2A $C\alpha$ -CFP along with pCMV5-small  $T_{WT}$ , pCMV5-small  $T_{MUT}$ , or empty vector. Co-transfection of BiFC constructs encoding YC- $A\alpha$  and YN-B56 $\gamma3$  or transfection of PP2A $C\alpha$ -CFP alone was used as a control for bleed-through. For visualizing PP2A  $A\alpha B55\beta2C\alpha$  holoenzyme complexes by BiFC-FRET analysis, NIH3T3 cells were transfected with BiFC constructs encoding YN- $A\alpha$  and PP2A $C\alpha$ -YC and a construct for B55 $\beta2_{WT}$ -CFP or B55 $\beta2_{MUT}$ -CFP with or without pCMV5-small  $T_{WT}$ , pCMV5-small  $T_{MUT}$ , or empty vector. Twenty-four hours after transfection, cells were fixed as described earlier, and visualized and analyzed by fluorescence microscopy (Zeiss, Axio observer Z1) equipped with the FRET three-filter set (Semrock), Ex 438/24, EM 483/32, and EM 542/27. The images were sequentially acquired by CFP, YFP, FRET<sub>CFP/YFP</sub> channels using image acquisition time ranging from 200 ms to 1000 ms which was kept constant for cells at random fields of different experimental groups. At least 10 cells of each set of experiments were individually measured for FRET images and corrected FRET intensity was obtained using Youvan's method [30] of AxioVision software. Each experiment was repeated at least two times.

## Results

### Immunofluorescence analysis of the subcellular distribution of individual PP2A subunits

We performed indirect immunofluorescence analyses to visualize the localization of Myc-tagged PP2A/ $A\alpha$  and HA-tagged PP2A $C\alpha$  in NIH3T3 cells. As shown in Fig. 1A, nearly 58% of the cells displayed a predominantly cytoplasmic expression pattern for both Myc-tagged PP2A/ $A\alpha$  and HA-tagged PP2A $C\alpha$  subunits, and approximately 35% of the cells displayed ubiquitous expression of these PP2A subunits. We also examined the localization pattern of various HA-tagged B subunits including B55 $\alpha$ , B55 $\beta1$ , B55 $\beta2$ , B55 $\delta$ , and B56 $\gamma3$  (Fig. 1C). B55 $\alpha$  and B55 $\delta$ , which share the highest sequence homology among B55 family members [31], showed mainly cytoplasmic distribution. B55 $\beta1$  was ubiquitously expressed in entire cells or predominantly cytoplasmic, but B55 $\beta2$  was mainly cytoplasmic. Consistent with a previous investigation that showed B55 $\beta2$ , but not B55 $\beta1$ , is located to mitochondria [9], we found that the distribution of B55 $\beta2$  was more

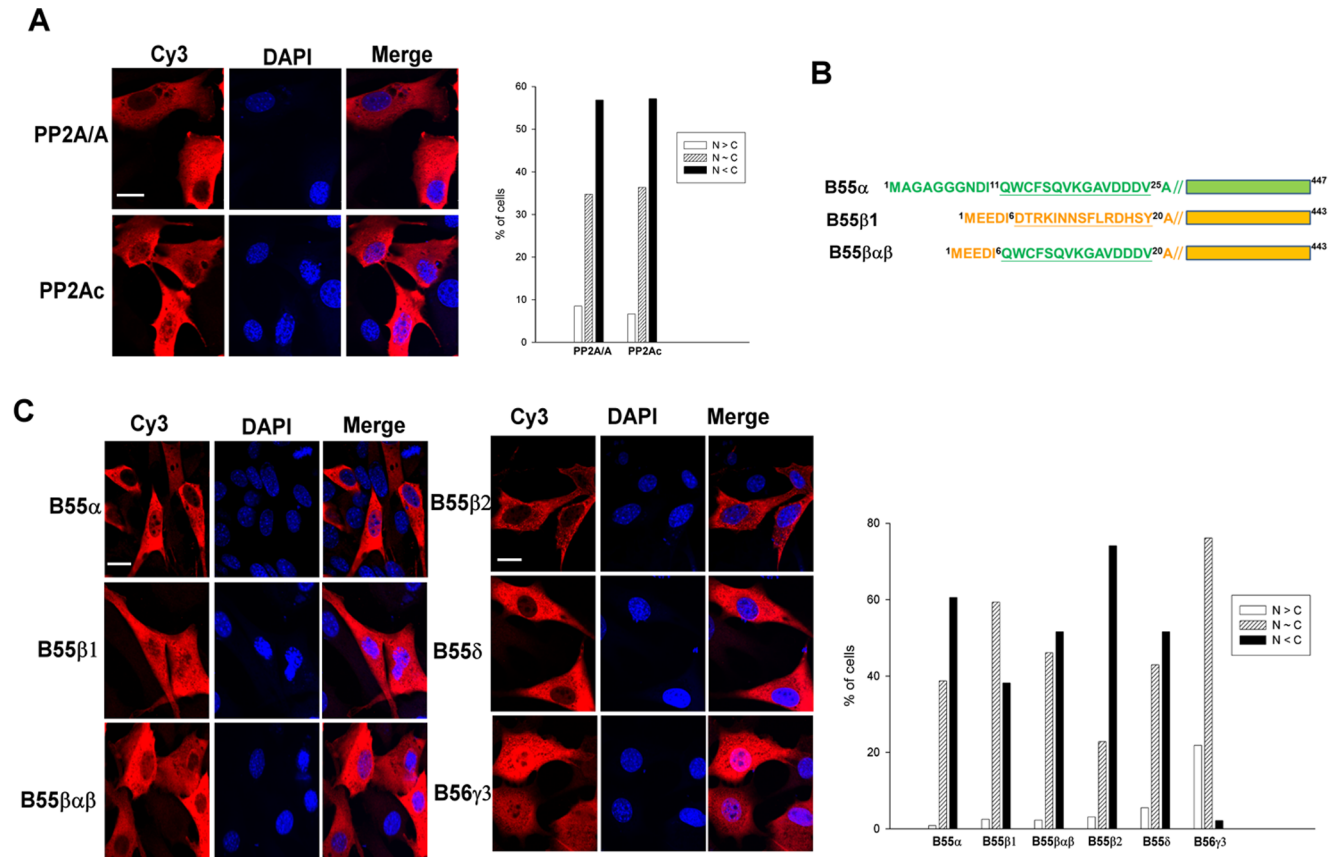


**Fig. 1. Subcellular distribution of PP2A subunits.** (A) NIH3T3 cells were transiently transfected with pCA2-6myc-PP2A/A $\alpha$  or pCMV-HA-PP2Ac $\alpha$ -YC, and expression of the exogenous A $\alpha$  and C $\alpha$  subunits was assessed by indirect immunofluorescence using anti-Myc tag and anti-HA antibodies, respectively, in conjunction with Cy3-conjugated secondary antibody. (B) Diagrams of B55 $\alpha$ , B55 $\beta$ , and the B55 $\beta\alpha\beta$  chimera mutant are shown. (C) NIH3T3 cells were transiently transfected with pcDNA3.1/Zeo(+)-B55 $\alpha$ -HA, pcDNA3.1/Zeo(+)-B55 $\beta$ -HA, pcDNA3.1/Zeo(+)-B55 $\beta\alpha\beta$ -HA, pcDNA3.1/Zeo(+)-B55 $\beta$ 2-HA, pcDNA3.1/Zeo(+)-B55 $\delta$ -HA, or pcDNA3.1/Zeo(+)-B56 $\gamma$ 3-HA. Expression of various exogenous B isoforms was assessed by indirect immunofluorescence using the anti-HA antibody and Cy3-conjugated secondary antibody. DAPI was applied for staining of nuclei. Scale bars: 20  $\mu$ m. Cells with different distribution patterns were scored as follows: predominantly nuclear (N>C), homogeneously distributed in both nucleus and cytoplasm (N~C), and predominantly cytoplasmic (N<C). Quantified data from one of at least two independent experiments with similar results are shown. At least 200 cells were counted for each group.

doi:10.1371/journal.pone.0116074.g001

punctate, which is a hallmark of mitochondrial localization. B56 $\gamma$ 3, which is a member of the B56 family of the regulatory subunits, was ubiquitously distributed in most of the cells and was highly enriched in the nucleus of a subset of cells. We also examined the localization of B55 $\beta\alpha\beta$ , which is a chimera of B55 $\beta$ 1 with amino acid residues 6 to 20 replaced by amino acid residues 11 to 25 of B55 $\alpha$  (Fig. 1B). As shown in Fig. 1C, the cytoplasmic distribution of B55 $\beta\alpha\beta$  was increased relative to that of wildtype B55 $\beta$ 1, and more closely resembled the distribution pattern of B55 $\alpha$ . This finding suggests that the very diverse region at the N-terminus of B55 $\alpha$  and B55 $\beta$ 1 plays a key role in regulating the subcellular targeting of these highly similar subunits. Together, in agreement with prior studies [9–11, 32], our immunofluorescence analyses of individual B subunits indicate that they display unique subcellular localization patterns.

## BiFC analysis of subunit interactions

To investigate the interaction of canonical PP2A subunits (e.g., A and C, A and B, and B and C), we exploited BiFC (Fig. 2A). Mammalian expression plasmids encoding A $\alpha$ , PP2Ac $\alpha$ , B55 $\alpha$ , B55 $\beta$ 1, B55 $\beta$ 2, B55 $\beta$  $\alpha$  $\beta$ , B55 $\delta$ , or B56 $\gamma$ 3 fused to an N-terminal fragment of yellow fluorescent protein (YN) or to a C-terminal fragment of yellow fluorescent protein (YC), at either the N terminus or C terminus of the PP2A subunit, were generated and transfected into NIH3T3 cells. The BiFC efficiency of paired YN- and YC-fused PP2A subunits was assessed by fluorescence microscopy. Our analysis of various pairs of YN- or YC-fused A $\alpha$  and PP2Ac $\alpha$  subunits revealed that the highest BiFC signals were generated from the combination of YN-A $\alpha$  and PP2Ac $\alpha$ -YC (Fig. 2B and S1 Fig.). In agreement with the results of indirect immunofluorescence of A $\alpha$  and PP2Ac $\alpha$  (Fig. 1A), the BiFC signals of YN-A $\alpha$ /PP2Ac $\alpha$ -YC complexes were mainly cytoplasmic in most cells; however, some cells exhibited fairly ubiquitous or nuclear-enriched localization of these complexes (Fig. 2B).

Next, we investigated the interactions between A and B subunits using BiFC. Our analyses of various pairs of YN- or YC-fused A $\alpha$  and B55 $\alpha$ , B55 $\beta$ 1, or B55 $\beta$  $\alpha$  $\beta$  subunits revealed that the highest BiFC signals were obtained from the combination of A $\alpha$ -YC or YC-A $\alpha$  and YN-B for all three tested B subunits (S2–S4 Figs.). Our BiFC studies revealed that A $\alpha$ -YC/YN-B55 $\alpha$ , A $\alpha$ -YC/YN-B55 $\beta$ 2, A $\alpha$ -YC/YN-B55 $\beta$  $\alpha$  $\beta$ , and A $\alpha$ -YC/YN-B55 $\delta$  complexes were mainly cytoplasmic, and to a much lesser extent, in a ubiquitous or in a nuclear-enriched manner (Fig. 2C). However, BiFC signals of A $\alpha$ -YC/YN-B55 $\beta$ 1 and YC-A $\alpha$ /YN-B56 $\gamma$ 3 complexes were mainly ubiquitous, but some cells exhibited highly nuclear-enriched BiFC signals for YC-A $\alpha$ /YN-B56 $\gamma$ 3 complexes (Fig. 2C). Moreover, consistent with the results of indirect immunofluorescence analysis of individual B subunits (Fig. 1C), A $\alpha$ -YC/YN-B55 $\beta$  $\alpha$  $\beta$  complexes displayed a more predominant cytoplasmic distribution than A $\alpha$ -YC/YN-B55 $\beta$ 1 complexes, which were ubiquitously distributed. This observation confirms that the divergent N-terminal regions of B55 $\alpha$  and B55 $\beta$  play an important role in regulating the subcellular targeting of two very similar subunits. Co-immunoprecipitation experiments not only verified that A $\alpha$ -YC or YC-A $\alpha$  can interact with the various YN-B subunits (S5 Fig.), but also demonstrated association of the endogenous PP2A/A and PP2Ac subunits with the YN-B subunits (S5 Fig.). These data indicate that the BiFC signals formed between fluorescent protein fragments fused with A and B subunits most likely represent the trimeric ABC holoenzyme complex.

We extended our BiFC analyses to explore interactions between the B and C subunit. We chose the B55 $\beta$ , B55 $\delta$  and B56 $\gamma$ 3 subunits for investigation because they showed higher BiFC signals than the other B subunits (Fig. 2C). No appreciable BiFC signals could be detected following expression of different pairs of YN- or YC-fused PP2Ac $\alpha$  and YN- or YC-fused B55 $\beta$ , B55 $\delta$  and B56 $\gamma$ 3 subunits (S6–S8 Figs.). However, marked BiFC signals were detected when A $\alpha$  was co-expressed with PP2Ac $\alpha$ -YC and either YN-B56 $\gamma$ 3 or YN-B55 $\beta$ 1 (Fig. 2D and S6–S7 Figs.). These findings verify that the A subunit functions as a scaffold for

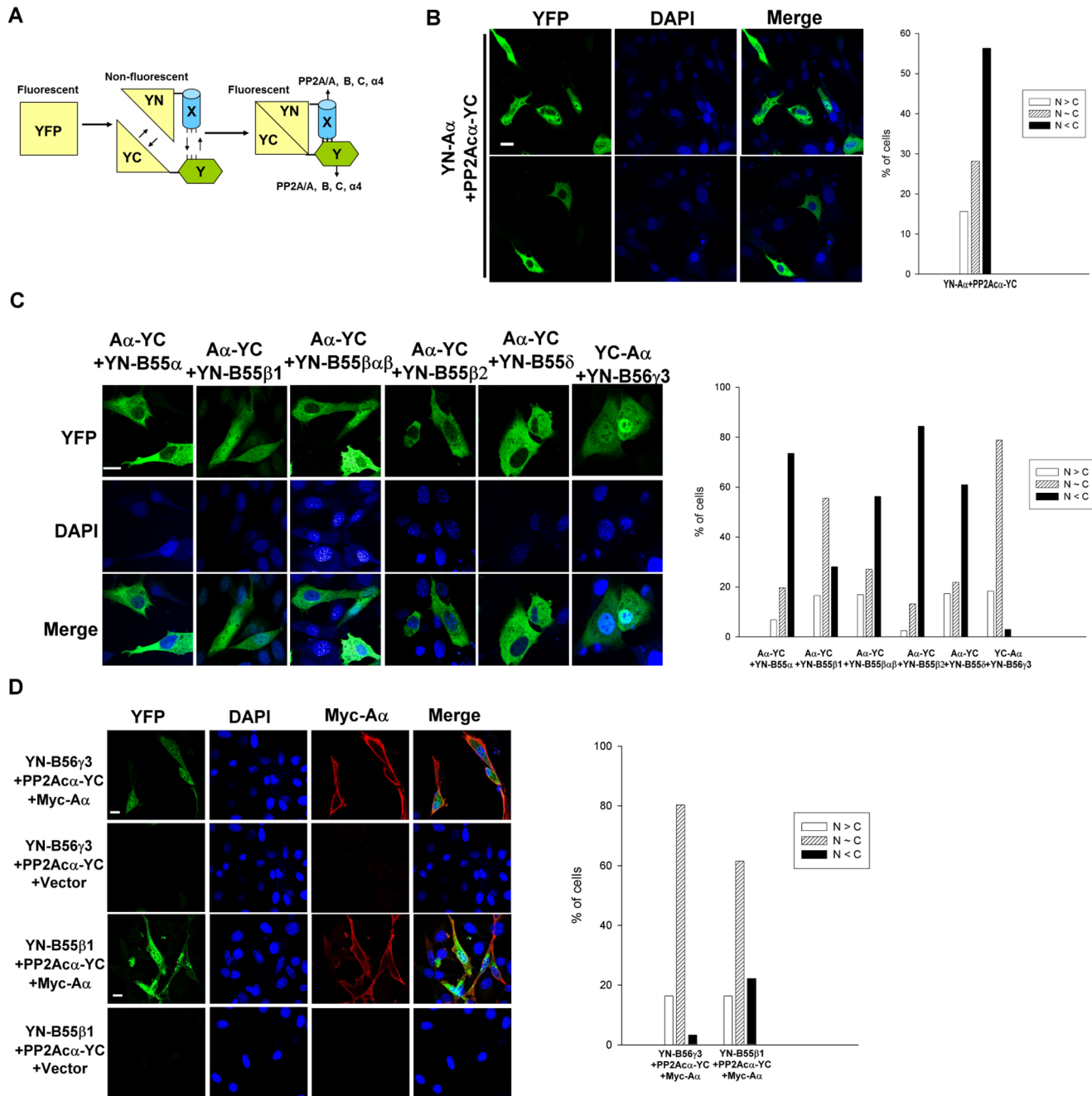


**Fig. 2. BiFC analysis enables visualization of association between two subunits of PP2A in cells.** (A) Design of BiFC analysis of dimeric interactions between PP2A subunits is shown. Fluorescence is regained when reconstitution of YFP from two fragments of YFP takes place due to an interaction between PP2A subunits fused to the fragments. (B) Equal amounts of BiFC expression constructs encoding YN-A $\alpha$  and PP2A $\alpha$ -YC were co-transfected into NIH3T3 cells. YFP signals due to BiFC of YN-A $\alpha$  and PP2A $\alpha$ -YC were measured by fluorescence microscopy. (C) Equal amounts of BiFC expression constructs encoding A $\alpha$ -YC and YN-B55 $\alpha$ , YN-B55 $\beta$ 1, YN-B55 $\beta$ 2, YN-B55 $\beta$ 3, or YN-B55 $\delta$ , or constructs encoding YC-A $\alpha$  and YN-B56 $\gamma$ 3 were transfected into NIH3T3 cells. YFP signals due to BiFC of A $\alpha$ -YC and YN-B were measured by fluorescence microscopy. (D) Equal amounts of BiFC expression constructs encoding PP2A $\alpha$ -YC and YN-B55 $\beta$ 1 or YN-B56 $\gamma$ 3 with or without equal amounts of pCA2-6myc-PP2A/A $\alpha$  were co-transfected into NIH3T3 cells, and 24 h after transfection, YFP signals due to BiFC of PP2A $\alpha$ -YC and YN-B55 $\beta$ 1 or YN-B56 $\gamma$ 3 were measured by direct fluorescence microscopy and expression of 6myc-PP2A/A $\alpha$  was confirmed by indirect immunofluorescence using anti-Myc tag antibody and Cy3-conjugated secondary antibody. DAPI was applied for staining of nuclei. Scale bars: 20  $\mu$ m. Graphs show quantitative analysis of distribution of BiFC signals in cells from one of at least two independent experiments with similar results, and at least 100 cells were assessed from several random fields. Cells with different distribution patterns of BiFC signals were scored as described earlier.

doi:10.1371/journal.pone.0116074.g002

the B and C subunits. The BiFC signals for PP2A $\alpha$ /B56 $\gamma$ 3 and PP2A $\alpha$ /B55 $\beta$ 1 in the presence of A $\alpha$  also showed distribution patterns similar to those observed for A $\alpha$ /B56 $\gamma$ 3 and A $\alpha$ /B55 $\beta$ 1 complexes, respectively (compare Fig. 2C, D). Although B55 $\delta$  shares high similarity with B55 $\beta$ , no obvious BiFC signals were detected in all combinations of YN- or YC-fused PP2A $\alpha$  and B55 $\delta$  regardless of whether or not A $\alpha$  was co-expressed (S8 Fig.). We also found no significant differences between the expression levels of YN-B55 $\beta$ 1 and YN-B55 $\delta$ , and association of PP2A $\alpha$ -YC with YN-B55 $\beta$ 1 and YN-B55 $\delta$  (S9 Fig.).

Since we previously showed that B56 $\gamma$ 3 is enriched in the nucleus at the G1 to S transition and at early S phase [29], we applied BiFC analysis to determine if complexes of A $\alpha$ /B56 $\gamma$ 3 were regulated in a similar fashion. Consistent with our prior study [29], immunofluorescence analysis revealed that, in comparison to asynchronous cells, B56 $\gamma$ 3 became highly enriched in the nucleus following cell synchronization at early S phase, whereas B55 $\alpha$  showed only a moderate increase in the nuclear distribution when cells were synchronized at early S phase (Fig. 3A). Likewise, we found that BiFC complexes of A $\alpha$ /B56 $\gamma$ 3 were homogeneously distributed in entire cells, but became highly enriched in the nucleus in cells synchronized at early S phase (Fig. 3B). In contrast, only a moderate increase in nuclear distribution of A $\alpha$ /B55 $\alpha$  BiFC complexes was found at early S phase as compared to that at steady state (Fig. 3B). Collectively, these results indicate that BiFC complexes of A and B subunits behave similarly to individual B subunits (Table 1). Together, these findings confirm that the A subunit functions as a scaffold for the B and C subunits, and demonstrate that the B subunit dictates the subcellular localization of canonical PP2A holoenzymes.

### SV40 small t antigen disrupts BiFC between A $\alpha$ and various B subunits

Since SV40 small t antigen (SMT) binds to the A subunit and displaces B subunits from PP2A heterotrimeric holoenzymes [33], we investigated whether SMT can disrupt BiFC complexes formed between A and B subunits. YC-A $\alpha$  and YN-B56 $\gamma$ 3 were co-expressed with wildtype SV40 small t antigen (SMT<sub>WT</sub>) or a mutant form of SV40 small t antigen (SMT<sub>MUT</sub>) defective in binding the A subunit [34]. Expression of SMT<sub>WT</sub>, but not the SMT<sub>MUT</sub>, abolished the BiFC signal generated from co-expression of YC-A $\alpha$  and YN-B56 $\gamma$ 3 (Fig. 4A). SMT<sub>WT</sub> also significantly attenuated the BiFC signals in cells expressing A $\alpha$ -YC and YN-B55 $\alpha$ , YN-B55 $\beta$ 1, YN-B55 $\beta$ 2, YN-B55 $\beta$  $\alpha$  $\beta$ , or YN-B55 $\delta$ , whereas SMT<sub>MUT</sub> did not affect the BiFC complexes (S10 Fig.). Results from co-immunoprecipitation experiments confirmed that SMT<sub>WT</sub>, but not SMT<sub>MUT</sub>, significantly disrupted the interaction of YN-B56 $\gamma$ 3 with A $\alpha$ -YC as well as with endogenous A $\alpha$  and C $\alpha$  subunits (Fig. 4B). These findings indicate that the BiFC signals detected following co-expression of A $\alpha$ -YC and various YN-fused B subunits are indeed due to specific

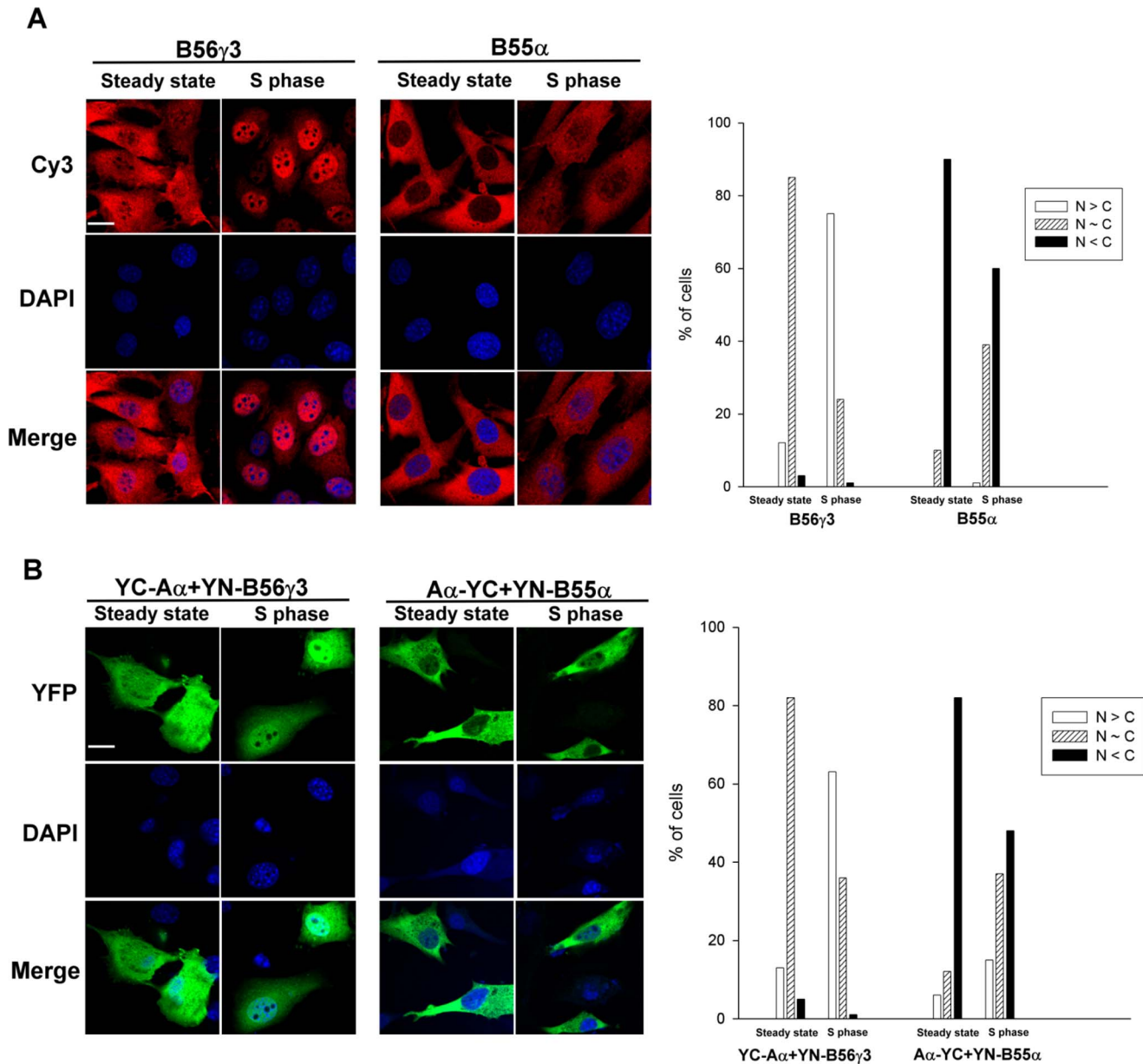


**Fig. 3. BiFC analysis confirms that B56 $\gamma$ 3, but not B55 $\alpha$ , promotes PP2A/A $\alpha$  accumulation in the nucleus in early S phase.** (A) NIH3T3 cells stably expressing HA-tagged B56 $\gamma$ 3 or B55 $\alpha$  were synchronized at the early S phase by double thymidine block treatment [48] followed by released in the regular medium for 3 h as described before [29]. Expression of B56 $\gamma$ 3 or B55 $\alpha$  was assessed by indirect immunofluorescence using anti-HA antibody in conjunction with Cy3-conjugated secondary antibody. (B) Equal amounts of BiFC expression constructs encoding YC-A $\alpha$  and YN-B56 $\gamma$ 3 or equal amounts of BiFC expression constructs encoding A $\alpha$ -YC and YN-B55 $\alpha$  were co-transfected into NIH3T3 cells. Twenty-four hour after transfection, cells were either treated with 10  $\mu$ g/ml aphidicolin or left untreated for 18 h and subsequently grown in fresh medium without aphidicolin treatment for 3 h, followed by direct fluorescence microscopy for imaging YFP signals due to BiFC of YC-A $\alpha$  and YN-B56 $\gamma$ 3 or BiFC of A $\alpha$ -YC and YN-B55 $\alpha$ . DAPI was applied for staining of nuclei. Scale bars, 20  $\mu$ m. Graphs show quantitative analysis of distribution of BiFC signals in cells from one of at least two independent experiments with similar results, and at least 100 cells were assessed from several random fields. Cells with different distribution patterns of BiFC signals were scored as described earlier.

doi:10.1371/journal.pone.0116074.g003

**Table 1.** Subcellular distribution of different subunits and BiFC complexes of PP2A.

Subunit	Location Major/secondary	Subunit	Location Major/secondary	BiFC complex	Location Major/secondary
A $\alpha$	Cytoplasmic/Ubiquitous	B55 $\alpha$	Cytoplasmic/Ubiquitous	A $\alpha$ /B55 $\alpha$	Cytoplasmic/Ubiquitous
		B55 $\beta$ 1	Ubiquitous/Cytoplasmic	A $\alpha$ /B55 $\beta$ 1	Ubiquitous/Cytoplasmic
		B55 $\beta$ $\alpha\beta$	Either Cytoplasmic or Ubiquitous	A $\alpha$ /B55 $\beta$ $\alpha\beta$	Cytoplasmic/Ubiquitous
		B55 $\beta$ 2	Cytoplasmic Punctate/Ubiquitous	A $\alpha$ /B55 $\beta$ 2	Cytoplasmic/Ubiquitous
		B55 $\delta$	Cytoplasmic/Ubiquitous	A $\alpha$ /B55 $\delta$	Cytoplasmic/Ubiquitous
C $\alpha$	Cytoplasmic/Ubiquitous	B56 $\gamma$ 3	Ubiquitous/Nuclear- enriched	A $\alpha$ /B56 $\gamma$ 3	Ubiquitous/Nuclear- enriched
		C $\alpha$	Cytoplasmic/Ubiquitous	A $\alpha$ /C $\alpha$	Cytoplasmic/Ubiquitous
		B55 $\beta$ 1	Ubiquitous/Cytoplasmic	C $\alpha$ /B55 $\beta$ 1	Ubiquitous/Cytoplasmic
		B56 $\gamma$ 3	Ubiquitous/Nuclear- enriched	C $\alpha$ /B56 $\gamma$ 3	Ubiquitous/Nuclear- enriched

doi:10.1371/journal.pone.0116074.t001

protein-protein interactions and not the result of spontaneous interactions between two non-fluorescent fragments of a split YFP.

### BiFC analysis of PP2A $\alpha$ 4 complexes

Given that BiFC can be utilized to detect dimeric interactions of canonical PP2A subunits (Fig. 2), we applied it to investigate a non-canonical PP2A complex, namely the PP2A $\alpha$ 4 complex. Indirect immunofluorescence revealed that both

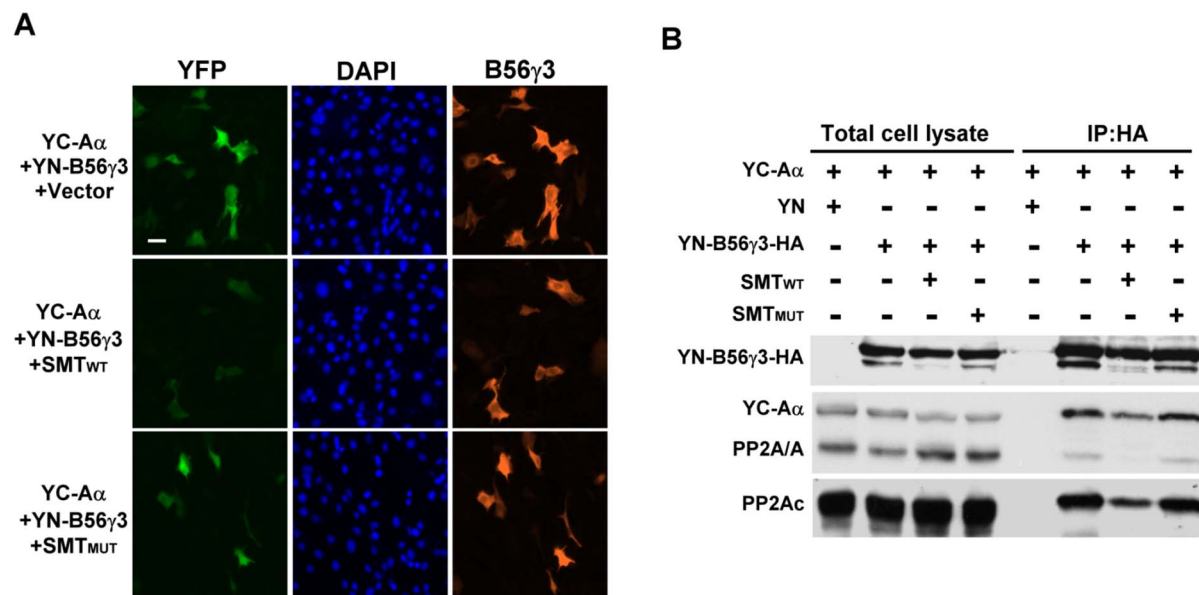


**Fig. 4. BiFC between YC-A $\alpha$  and YN-B56 $\gamma$ 3 is disrupted by SV40 SMT.** (A) BiFC expression constructs encoding YC-A $\alpha$  and YN-B56 $\gamma$ 3 in the presence of pCMV5-SMT<sub>WT</sub>, -SMT<sub>MUT</sub>, or empty vector were transfected into NIH3T3 cells, and 24 h after transfection, YFP signals due to BiFC of YC-A $\alpha$  and YN-B56 $\gamma$ 3 were measured by fluorescence microscopy. Expression of HA-tagged YN-B56 $\gamma$ 3 was confirmed using anti-HA antibody as described earlier. (B) BiFC expression constructs encoding YC-A $\alpha$  and YN-B56 $\gamma$ 3 in the presence of pCMV5 SMT<sub>WT</sub>, -SMT<sub>MUT</sub>, or empty vector were transfected into NIH3T3 cells. Cell lysates were collected 24 h post-transfection, and immunoprecipitation was performed using anti-HA-Sepharose. The cell lysates and anti-HA immunocomplexes were then analyzed by SDS-PAGE and Western blotting using indicated antibodies.

doi:10.1371/journal.pone.0116074.g004

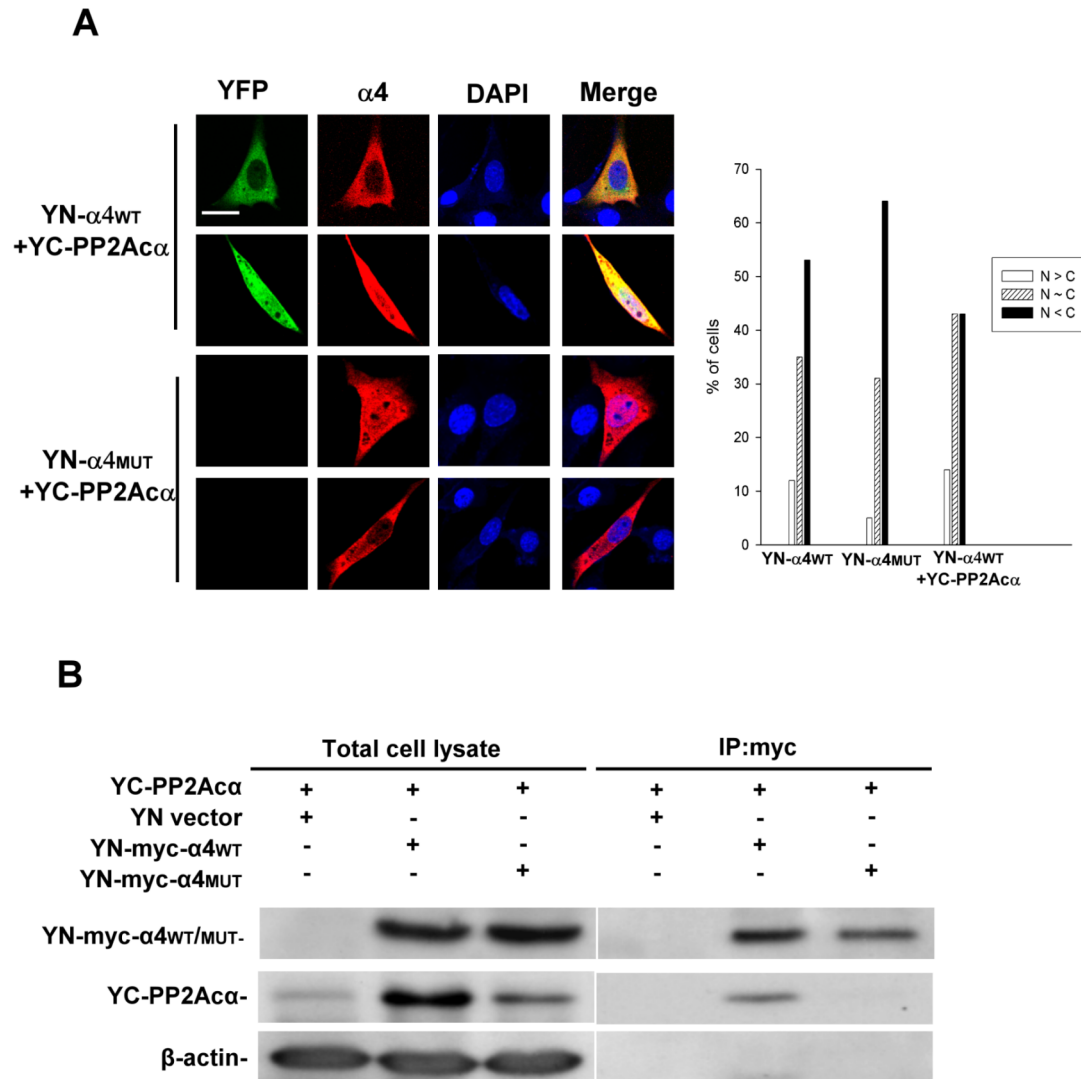


**Fig. 5. Visualization of the  $\alpha$ 4/PP2Ac complex by BiFC.** (A) BiFC expression constructs encoding YN- $\alpha$ 4<sub>WT</sub> or YN- $\alpha$ 4<sub>MUT</sub> and YC-PP2Ac $\alpha$  were transfected into NIH3T3 cells. YFP signals due to BiFC of YN- $\alpha$ 4<sub>WT</sub> or BiFC of YN- $\alpha$ 4<sub>MUT</sub> and YC-PP2Ac $\alpha$  were measured by fluorescence microscopy. Expression of Myc-tagged YN- $\alpha$ 4<sub>WT</sub> or YN- $\alpha$ 4<sub>MUT</sub> was confirmed using anti-Myc antibody in conjunction with Cy3-conjugated secondary antibody by indirect immunofluorescence microscopy. DAPI was applied for staining of nuclei. Scale bars: 20  $\mu$ m. Cells with different distribution patterns were scored as described earlier. Quantified data from one of at least two independent experiments with similar results are shown. At least 150 cells were counted for each group. (B) BiFC expression constructs encoding YN- $\alpha$ 4<sub>WT</sub> or YN- $\alpha$ 4<sub>MUT</sub> and YC-PP2Ac $\alpha$  were transfected into NIH3T3 cells. Cell lysates were collected 24 h post-transfection and immunoprecipitations were performed using anti-Myc tag antibody. The cell lysates and anti-Myc tag immunocomplexes were then analyzed by SDS-PAGE and Western blotting using the indicated antibodies.

doi:10.1371/journal.pone.0116074.g005

YN-tagged wildtype alpha4 ( $\alpha$ 4<sub>WT</sub>) and a mutant alpha4 defective in PP2Ac binding ( $\alpha$ 4<sub>MUT</sub>) [35, 36] were distributed in a primarily cytoplasmic manner and, to a lesser extent, in a ubiquitous manner (Fig. 5A,  $\alpha$ 4 panels). Co-expression of YN- $\alpha$ 4<sub>WT</sub> and YC-PP2Ac $\alpha$  resulted in significant BiFC signals, whereas no apparent BiFC signals were detected when the YN- $\alpha$ 4<sub>MUT</sub> was co-expressed with YC-PP2Ac $\alpha$  (Fig. 5A, YFP panels). Like the expression pattern of PP2Ac (Fig. 1) and  $\alpha$ 4 observed by immunofluorescence (Figs. 1 and 5A), the subcellular

distribution of YC-PP2A $\alpha$ /YN- $\alpha$ <sub>4</sub><sup>WT</sup> complexes was either ubiquitous or mainly cytoplasmic, and to a much lesser extent, nuclear-enriched (Fig. 5A, graph). To verify the YN- $\alpha$ <sub>4</sub>/YC-PP2A $\alpha$  BiFC data, we performed co-immunoprecipitation experiments. As shown in Figure 5B, YN- $\alpha$ <sub>4</sub><sup>WT</sup>, but not YN- $\alpha$ <sub>4</sub><sup>MUT</sup>, associated with YC-PP2A $\alpha$ .

The  $\alpha$ <sub>4</sub> and A subunits directly associate with C subunit in a mutually exclusive fashion and  $\alpha$ <sub>4</sub> appears to compete with the A subunit for binding the C subunit [13, 14]. To test the competition hypothesis using BiFC, we co-expressed YN-A $\alpha$  and PP2A $\alpha$ -YC together with or without  $\alpha$ <sub>4</sub>. Surprisingly, we found that co-expression of  $\alpha$ <sub>4</sub><sup>WT</sup> resulted in increased BiFC signals of YN-A $\alpha$ /PP2A $\alpha$ -YC complexes (Fig. 6A). The increased YN-A $\alpha$ /PP2A $\alpha$ -YC BiFC signals were not observed when the PP2Ac binding-defective mutant of  $\alpha$ <sub>4</sub> was introduced into the cells (Fig. 6A). The  $\alpha$ <sub>4</sub>-induced increases in YN-A $\alpha$ /PP2A $\alpha$ -YC BiFC signals were further verified by co-immunoprecipitation and Western blotting analysis. These experiments revealed that co-expression of  $\alpha$ <sub>4</sub><sup>WT</sup>, but not  $\alpha$ <sub>4</sub><sup>MUT</sup>, resulted in increased levels of PP2A $\alpha$ -YC protein without affecting the levels of YN-A $\alpha$  or endogenous A $\alpha$  and PP2A $\alpha$  (Fig. 6B). Consistent with the BiFC analysis, more complexes formed between PP2A $\alpha$ -YC and YN-A $\alpha$  or endogenous A $\alpha$  in the presence of  $\alpha$ <sub>4</sub><sup>WT</sup> compared to that in the presence of vector or  $\alpha$ <sub>4</sub><sup>MUT</sup> (Fig. 6B). These findings demonstrate that  $\alpha$ <sub>4</sub> may not act as a competitor of the A subunit for binding PP2Ac in cells, but instead likely plays a protective role in stabilizing newly synthesized free C subunits prior to formation of a stable AC core enzyme complex [17, 21].

### Visualization of the trimeric PP2A holoenzyme complexes

The PP2A heterotrimeric holoenzymes are the predominant forms of PP2A in cells, and have been purified from a number of different tissues and cell lines [4, 37, 38]. However, direct visualization of the holoenzyme complexes in cells has hitherto not been reported. After successfully utilizing BiFC to observe the association of two individual PP2A subunits in cells (Fig. 2), we next employed BiFC-FRET to visualize the trimeric PP2A holoenzyme complexes in cells (Fig. 7A). We first investigated the trimeric A $\alpha$ /B56 $\gamma$ 3/C $\alpha$  complex by co-expressing YC-A $\alpha$  and YN-B56 $\gamma$ 3, which serves as a FRET acceptor when YFP is reconstituted via BiFC of YC-A $\alpha$ /YN-B56 $\gamma$ 3, together with CFP-PP2A $\alpha$ , which serves as a FRET donor (Fig. 7A). As shown in Figure 7B, FRET occurred following co-expression of YC-A $\alpha$ , YN-B56 $\gamma$ 3, and CFP-PP2A $\alpha$ , but no FRET was observed in cells expressing YC-A $\alpha$ , YN-empty vector, and CFP-PP2A $\alpha$ . These findings indicate that the YC-A $\alpha$ /YN-B56 $\gamma$ 3/CFP-PP2A $\alpha$  heterotrimer can be formed in cells. The FRET mainly displayed a homogenous pattern throughout the entire cell, which is similar to the distribution patterns of B56 $\gamma$ 3 (Fig. 1B) and BiFC complexes of A $\alpha$ /B56 $\gamma$ 3 and B56 $\gamma$ 3/PP2A $\alpha$  (Fig. 2C). The specificity of FRET between YC-A $\alpha$ /YN-B56 $\gamma$ 3 and CFP-PP2A $\alpha$  was further verified by co-expression of SV40 SMT<sup>WT</sup> or SMT<sup>MUT</sup>. Co-expression of SMT<sup>WT</sup> abolished both BiFC (YFP) of the YC-A $\alpha$ /YN-B56 $\gamma$ 3 complex and FRET between the BiFC

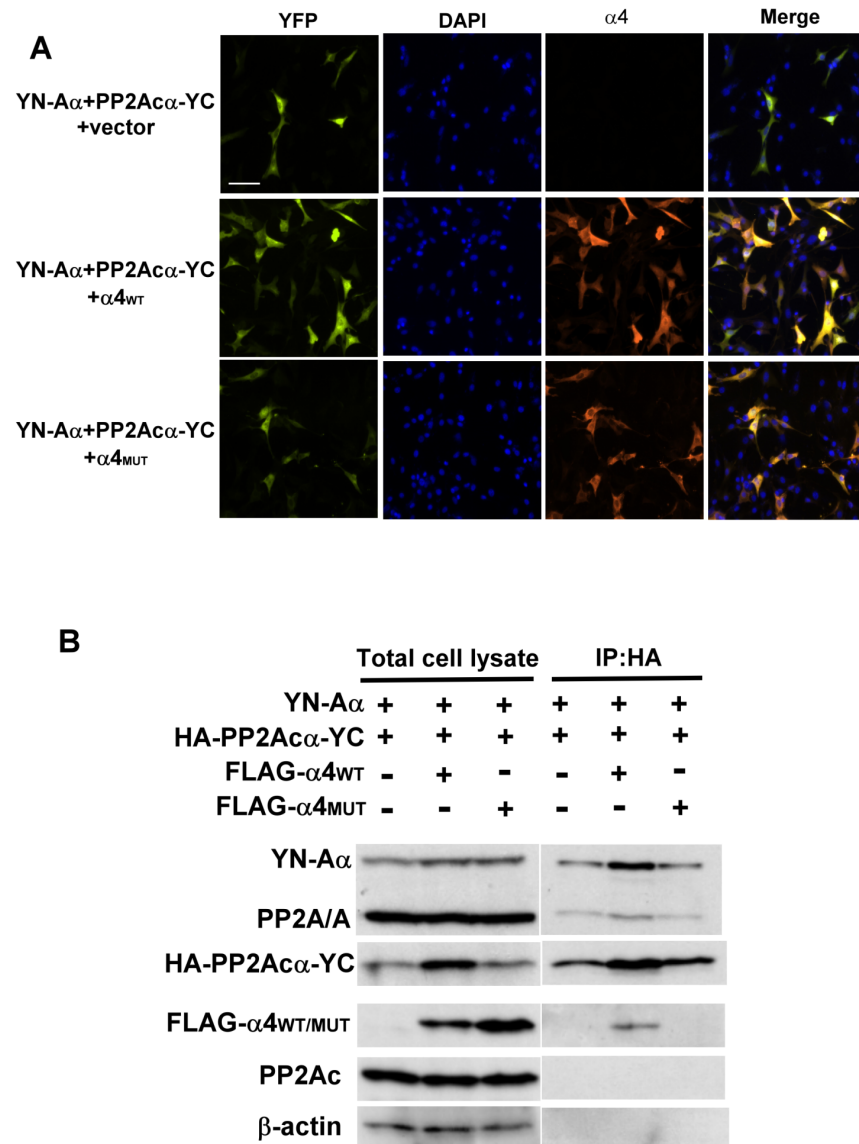


**Fig. 6.  $\alpha 4$  facilitates formation of PP2A AC core enzyme.** (A) Equal amounts of BiFC expression constructs encoding YN-A $\alpha$  and PP2Ac $\alpha$ -YC in the presence of equal amounts of pcDNA5/To-Flag- $\alpha 4_{WT}$ , pcDNA5/To-Flag- $\alpha 4_{MUT}$ , or empty vector were transfected into NIH3T3 cells. YFP signals due to BiFC of YN-A $\alpha$  and PP2Ac $\alpha$ -YC were measured by fluorescence microscopy. Expression of Flag- $\alpha 4_{WT}$  or Flag- $\alpha 4_{MUT}$  was verified using anti-FLAG antibody and Cy3-conjugated secondary antibody. DAPI was applied for staining of nuclei. Scale bars, 20  $\mu$ m. (B) BiFC expression constructs encoding YN-A $\alpha$  and HA-PP2Ac $\alpha$ -YC and pcDNA5/To-Flag- $\alpha 4_{WT}$ , pcDNA5/To-Flag- $\alpha 4_{MUT}$ , or empty vector were transfected into NIH3T3 cells. Cell lysates were collected 24 h post-transfection, and immunoprecipitations were performed using anti-HA Sepharose. The cell lysates and anti-HA immunocomplexes were then analyzed by SDS-PAGE and Western blotting using the indicated antibodies.

doi:10.1371/journal.pone.0116074.g006

complex of YC-A $\alpha$ /YN-B56 $\gamma 3$  and CFP-PP2Ac $\alpha$ , but both BiFC (YFP) and FRET were retained when SMT<sub>MUT</sub> was co-expressed (Fig. 7B).

To further establish the feasibility of using BiFC-FRET to visualize heterotrimeric PP2A complexes, we applied this method to visualize the A $\alpha$ /

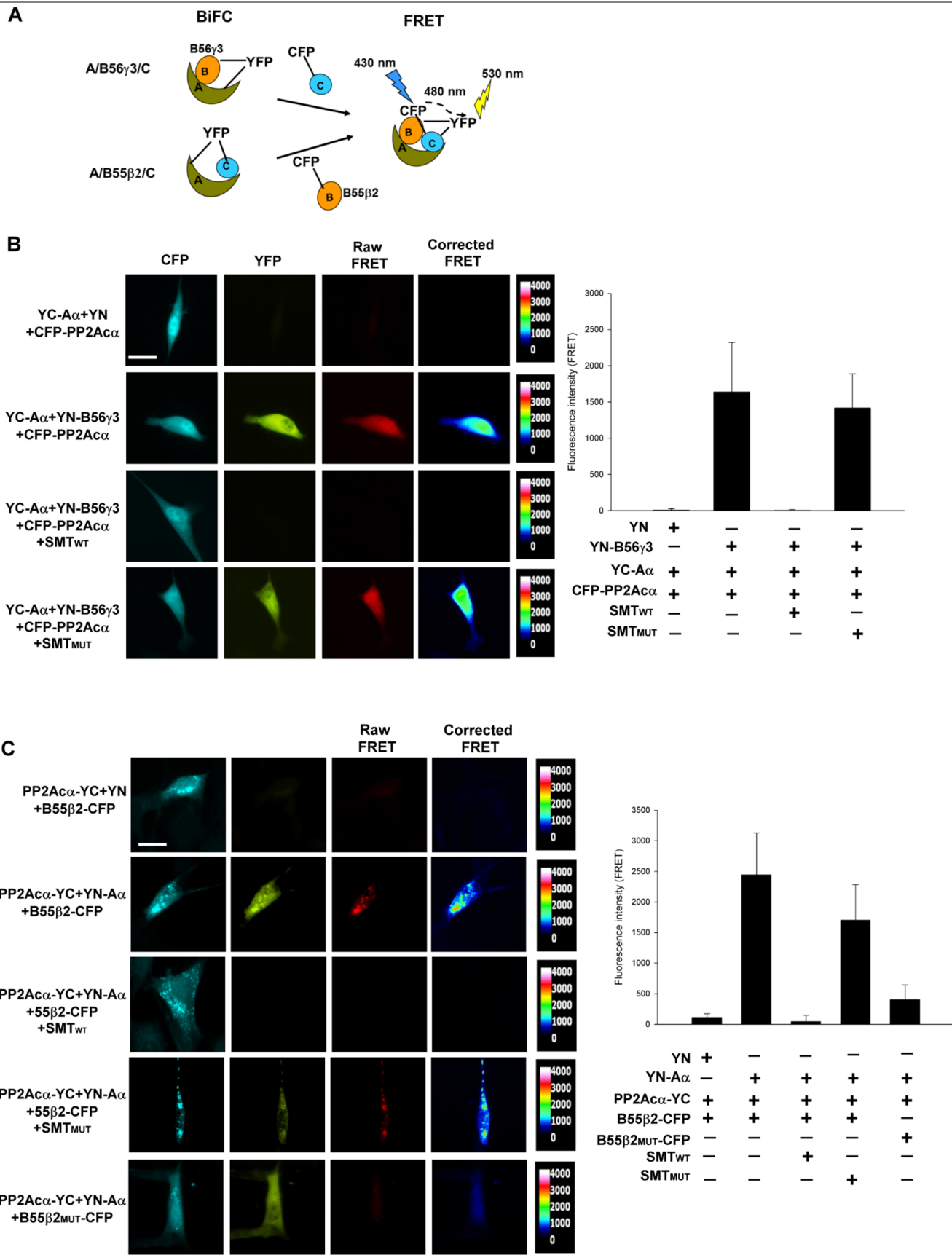


**Fig. 7. Visualization of the PP2A trimeric holoenzyme complexes  $A\alpha/B56\gamma3/C\alpha$  and  $A\alpha/B55\beta2/C\alpha$  in cells by BiFC-FRET.** (A) The design of BiFC-FRET analysis of  $A\alpha/B56\gamma3/C\alpha$  and  $A\alpha/B55\beta2/C\alpha$  is shown. YFP, which serves as a FRET acceptor, is reconstituted via BiFC of YC- $A\alpha$ /YN-B56 $\gamma3$  or PP2A $\alpha$ -YC/YN- $A\alpha$ , in ternary complex  $A\alpha/B56\gamma3/C\alpha$  or  $A\alpha/B55\beta2/C\alpha$ , respectively. FRET occurs when CFP-PP2A $\alpha$  or B55 $\beta2$ -CFP, which serves as a FRET donor, associates with YC- $A\alpha$ /YN-B56 $\gamma3$  or YN- $A\alpha$ /PP2A $\alpha$ -YC BiFC complex, respectively. (B) NIH3T3 cells were transiently transfected with constructs encoding YC- $A\alpha$ , CFP-PP2A $\alpha$  and YN-vector or YN-B56 $\gamma3$ , in the presence of pCMV5-SMT<sub>WT</sub>, pCMV5-SMT<sub>MUT</sub>, or empty vector. Images of expression of CFP-PP2A $\alpha$ , YFP (due to BiFC of YC- $A\alpha$  and YN-B56 $\gamma3$ ), and FRET between CFP and YFP were acquired by indicated filters. Corrected FRET images were generated and FRET intensity was assessed by AxioVision (Zeiss), as described in the “[Methods and Materials](#)”. Representative images are shown. Scale bars, 20  $\mu$ m. Quantified data from one of two independent experiments with similar results are shown. Mean ( $\pm$  s.d.) of corrected FRET maximum intensity values of individual cells from at least 15 cells were measured for each group. (C) NIH3T3 cells were transiently transfected with constructs encoding PP2A $\alpha$ -YC and YN-vector or YN- $A\alpha$ , and B55 $\beta2$ -CFP in the presence of pCMV5-SMT<sub>WT</sub>, pCMV5-SMT<sub>MUT</sub>, or empty vector, or transfected with equal amounts of constructs harboring PP2A $\alpha$ -YC, YN- $A\alpha$ , and B55 $\beta2$ <sub>MUT</sub>-CFP. Representative images of expression of B55 $\beta2$ -CFP and B55 $\beta2$ <sub>MUT</sub>-CFP, YFP (due to BiFC of association of PP2A $\alpha$ -YC and YN- $A\alpha$ ), and FRET between CFP and YFP were acquired by indicated filters as described above. Scale bars: 20  $\mu$ m. Corrected FRET images were generated and FRET intensity was assessed as described earlier. Quantified data from one of two independent experiments with similar results are shown. At least 10 cells were measured for each group.

doi:10.1371/journal.pone.0116074.g007

B55 $\beta2/C\alpha$  complex. We co-expressed PP2A $\alpha$ -YC and YN- $A\alpha$ , which serves as a FRET acceptor when YFP is reconstituted via BiFC of PP2A $\alpha$ -YC/YN- $A\alpha$ , together with B55 $\beta2$ -CFP, which serves as a FRET donor ([Fig. 7A](#)). As shown in [Figure 7C](#), FRET occurred when PP2A $\alpha$ -YC, YN- $A\alpha$ , and B55 $\beta2$ -CFP were co-expressed, and the pattern of FRET was largely punctate, similar to the distribution of B55 $\beta2$ -CFP ([Fig. 7C](#)), which is known to be a mitochondrially targeting subunit of PP2A [[9](#)]. The FRET was specific because co-expression of SMT<sub>WT</sub>, but not SMT<sub>MUT</sub>, along with PP2A $\alpha$ -YC, YN- $A\alpha$ , and B55 $\beta2$ -CFP resulted in no FRET ([Figure 7C](#)). In addition, we verified distribution pattern of  $A\alpha/B55\beta2/C\alpha$  by applying a mutant B55 $\beta2$ <sub>MUT</sub> (RR168EE) [[9](#)], which is defective in binding with the A subunit. When B55 $\beta2$ <sub>MUT</sub>-CFP was co-expressed with PP2A $\alpha$ -YC and YN- $A\alpha$ , FRET did not occur ([Fig. 7C](#)), suggesting that the observed FRET was specifically due to formation of a ternary YN- $A\alpha$ /B55 $\beta2$ -CFP/PP2A $\alpha$ -YC complex. Together, these results demonstrate that the PP2A holoenzyme complexes, such as  $A\alpha/B56\gamma3/C\alpha$  and  $A\alpha/B55\beta2/C\alpha$ , can be visualized in cells by BiFC-FRET.

## Discussion

In this report, we utilized BiFC analysis to investigate dimeric interactions between canonical PP2A subunits (A, B, and C), and successfully visualized most of the possible dimeric complexes formed by these subunits in cells. We also employed BiFC to visualize non-canonical PP2A $\alpha$ - $\alpha4$  interactions. Furthermore, we employed BiFC-FRET to visualize two different heterotrimeric PP2A holoenzymes in cells. Our findings demonstrate that these fluorescence-based methods can be utilized to study interactions between subunits of both canonical and non-canonical PP2A complexes in cells.

The strengths of BiFC include high sensitivity, high signal-to-background ratio, and high spatial resolution of protein-protein interactions in intact cells [[23](#)]. Our BiFC analyses revealed differences in the subcellular localization of various B isoform-containing A/B complexes, which were markedly similar to the subcellular distribution patterns of individual B subunits ([Figs. 1](#) and [2](#)). Not

surprisingly, BiFC analysis of B55 $\beta$  $\alpha$  $\beta$  (Fig. 1B), a domain swap mutant of B55 $\beta$ 1 harboring 15 amino acids of B55 $\alpha$ , also revealed a role for the highly divergent N-termini of B55 $\alpha$  and B55 $\beta$ 1 in determining the subcellular localization of these two highly related isoforms. In addition, BiFC analysis revealed that B56 $\gamma$ 3, but not B55 $\alpha$ , directed the A subunit to accumulate in the nucleus at the early S phase, which is consistent with our prior immunofluorescence and biochemical fractionation studies of individual subunits [29]. Our current findings not only demonstrate the high efficacy of using BiFC to assess the spatial distribution of dimeric interactions between PP2A subunits, but also provide the first direct imaging evidence indicating that the B subunit controls the subcellular localization of the PP2A holoenzyme.

The crystal structure of the trimeric PP2A A $\alpha$ /B56 $\gamma$ /PP2Ac $\alpha$  complex demonstrated extensive interactions between B56 $\gamma$  and PP2Ac $\alpha$  subunits [39, 40], but our BiFC analysis of PP2Ac $\alpha$  association with B55 $\beta$ 1, B55 $\delta$ , or B56 $\gamma$ 3 showed that the interaction between the B and PP2Ac $\alpha$  subunits is relatively inefficient without co-expression of the A subunit (S6–S8 Figs. and Fig. 2D). Co-expression of A $\alpha$  markedly facilitated BiFC complexes formed between B55 $\beta$ 1 or B56 $\gamma$ 3 and PP2Ac $\alpha$  subunits (S6–S8 Figs. and Fig. 2D). The inefficient association between PP2Ac $\alpha$ -YC and YN-B subunits in the absence of ectopically-expressed A $\alpha$  may be partly attributed to limited availability of endogenous A subunit, as the levels of endogenous PP2A A and C subunits are known to be tightly controlled in mammalian cells [41–43]. The ectopic A $\alpha$  likely promotes the assembly of the ternary complex when endogenous A subunits are limiting.

The presence of the fluorescent protein fragment at the C-terminus of PP2Ac $\alpha$ -YC may prevent it from undergoing carboxymethylation, which is required for the recruitment of some B subunits [22], especially B55 family members, into the holoenzyme complex. Given that the non-carboxymethylated PP2Ac $\alpha$  exhibits lower affinity for select B subunits [44], it is possible that the near irreversible association of two halves of YFP [23] helps tether the PP2Ac $\alpha$ -YC and YN-B subunits in the presence of ectopic A $\alpha$  subunit. In addition, it is possible that the binding to YN-A $\alpha$  stabilizes the conformation of non-carboxymethylated PP2Ac $\alpha$ -YC to increase the binding affinity for B55 subunits. Although B55 $\delta$  shares 83% identity with B55 $\beta$ 1, in contrast to B55 $\beta$ 1, no PP2Ac $\alpha$ /B55 $\delta$  BiFC complexes were found regardless of whether or not A $\alpha$  was co-expressed. The inability to detect PP2Ac $\alpha$ /B55 $\delta$  BiFC complexes could be the result of an unfavorable conformation for reconstituting fluorophore when PP2Ac $\alpha$  associates with B55 $\delta$ , since no obvious differences in expression levels of YN-B55 $\beta$ 1 and YN-B55 $\delta$  were detected, and YN-B55 $\delta$  was found to bind as efficiently as YN-B55 $\beta$ 1 to HA-PP2Ac $\alpha$ -YC (S9 Fig.). Our collective studies clearly demonstrate the scaffolding role of the A subunit in recruiting B and C subunits to form a mature PP2A holoenzyme.

In addition to the canonical PP2A trimeric holoenzyme complex, we were able to visualize non-canonical PP2Ac $\alpha$ / $\alpha$ 4 complexes in cells by BiFC (Fig. 5). Our results demonstrate increased formation of dimeric AC complexes in the presence of  $\alpha$ 4, which can be attributed to elevated PP2Ac levels following  $\alpha$ 4

overexpression (Fig. 6). These findings are in agreement with the PP2Ac stabilizing role of  $\alpha 4$  [17, 19–21].

BiFC and FRET have both been used to detect protein-protein interactions and visualize the localization of protein complexes in cells [23, 25]. Since the formation of PP2A complexes is postulated to be highly dynamic [22], we coupled BiFC with FRET, which measures instantaneous association and dissociation of multi-molecules [25, 45]. The combination of BiFC and FRET (BiFC-FRET) [27] allowed us to visualize two PP2A complexes in cells. The FRET signal for YC-A $\alpha$ /YN-B56 $\gamma 3$ /CFP-PP2Ac $\alpha$  complexes closely mirrored the immunostaining pattern of B56 $\gamma 3$  (compare Fig. 7B and Fig. 1C), with the highest FRET found surrounding and in the nucleus, which is consistent with prior reports showing that a subset of B56 $\gamma 3$  is localized to the Golgi apparatus or enriched in the nucleus [11, 29, 46] (Fig. 7B). In contrast, the FRET signal for YN-A $\alpha$ /B55 $\beta 2$ -CFP/PP2Ac $\alpha$ -YC complexes displayed a punctate, mitochondria-like distribution pattern. SV40 SMT is thought to displace the B subunit from the holoenzyme by binding to common HEAT repeats of the A subunit [34, 47]. Interestingly, we found that SV40 SMT also disrupts the BiFC between YN-A $\alpha$  and PP2Ac $\alpha$ -YC (Fig. 7C). Since SV40 SMT forms stable complexes with the AC core enzyme [47], we propose that the SMT-induced conformational change of the AC core enzyme is different from that made following B55 $\beta 2$  binding, which does not disrupt the BiFC between YN-A $\alpha$  and PP2Ac $\alpha$ -YC (Fig. 7C).

PP2A regulates myriad cellular functions, which is owing to the structural complexity of the PP2A holoenzymes. The holoenzyme complexes are thought to act on their substrates in a spatial and temporal manner, and are proposed to dynamically assemble and disassemble its components in response to environmental cues. Efforts to confirm prior models of PP2A regulatory processes have been hampered by the lack of tools to visualize distinct PP2A holoenzymes in cells. In this report, we demonstrate the successful application of BiFC-FRET to visualize two PP2A holoenzyme complexes in cells. We anticipate that this approach can be promptly applied to monitor changes in the localization of specific PP2A holoenzymes in real time. Moreover, by assessing the FRET of various ternary complexes (e.g., YC-PP2Ac/YN-A/B-CFP), we believe that this approach will allow us to study the dynamics of B subunit assembly with the AC core enzyme.

## Conclusions

BiFC was used to provide the first direct cell imaging evidence that the regulatory B subunit dictates the subcellular localization of the PP2A heterotrimeric holoenzyme, and that the A subunit functions as a scaffolding protein for assembly of a holoenzyme. In addition, our BiFC analyses indicate that  $\alpha 4$  may not act as a competitor of the A subunit for binding C subunits in cells, but instead stabilizes newly synthesized free C subunits for subsequent integration into active AC or ABC complexes. The BiFC-FRET system is a promising

approach for visualizing real-time dynamics of the subcellular distribution of individual PP2A holoenzymes in live cells.

## Supporting Information

**S1 Fig. BiFC analysis of various combinations of paired BiFC expression constructs encoding YN- or YC-fused A $\alpha$  and YC- or YN-fused PP2A $\alpha$ .** Equal amounts of BiFC expression constructs encoding YN- or YC-fused A $\alpha$  and YC- or YN-fused PP2A $\alpha$  were co-transfected into NIH3T3 cells, and 24 h after transfection, YFP signals due to BiFC of paired YN- or YC-fused A $\alpha$  and PP2A $\alpha$  were measured by fluorescence microscopy. DAPI was applied for staining of nuclei. Scale bar: 50  $\mu$ m.

[doi:10.1371/journal.pone.0116074.s001](https://doi.org/10.1371/journal.pone.0116074.s001) (PDF)

**S2 Fig. BiFC analysis of various combinations of paired BiFC expression constructs encoding YN- or YC-fused A $\alpha$  and YC- or YN-fused B55 $\alpha$ .** Equal amounts of BiFC expression constructs encoding YN- or YC-fused A $\alpha$  and YC- or YN-fused B55 $\alpha$  were co-transfected into NIH3T3 cells, and 24 h after transfection, YFP signals due to BiFC of paired YN- or YC-fused A $\alpha$  and B55 $\alpha$  were measured by fluorescence microscopy. DAPI was applied for staining of nuclei. Scale bar: 50  $\mu$ m.

[doi:10.1371/journal.pone.0116074.s002](https://doi.org/10.1371/journal.pone.0116074.s002) (PDF)

**S3 Fig. BiFC analysis of various combinations of paired BiFC expression constructs encoding YN- or YC-fused A $\alpha$  and YC- or YN-fused B55 $\beta$ 1.** Equal amounts of BiFC expression constructs encoding YN- or YC-fused A $\alpha$  and YC- or YN-fused B55 $\beta$ 1 were co-transfected into NIH3T3 cells, and 24 h after transfection, YFP signals due to BiFC of paired YN- or YC-fused A $\alpha$  and B55 $\beta$ 1 were measured by fluorescence microscopy. DAPI was applied for staining of nuclei. Scale bar: 50  $\mu$ m.

[doi:10.1371/journal.pone.0116074.s003](https://doi.org/10.1371/journal.pone.0116074.s003) (PDF)

**S4 Fig. BiFC analysis of various combinations of paired BiFC expression constructs encoding YN- or YC-fused A $\alpha$  and YC- or YN-fused B55 $\beta$  $\alpha$  $\beta$ .** Equal amounts of BiFC expression constructs encoding YN- or YC-fused A $\alpha$  and YC- or YN-fused B55 $\beta$  $\alpha$  $\beta$  were co-transfected into NIH3T3 cells, and 24 h after transfection, YFP signals due to BiFC of paired YN- or YC-fused A $\alpha$  and B55 $\beta$  $\alpha$  $\beta$  were measured by fluorescence microscopy. DAPI was applied for staining of nuclei. Scale bar: 50  $\mu$ m.

[doi:10.1371/journal.pone.0116074.s004](https://doi.org/10.1371/journal.pone.0116074.s004) (PDF)

**S5 Fig. Co-immunoprecipitation of BiFC complexes of PP2A/A $\alpha$  and various B subunits.** (A) Lysates of NIH3T3 cells co-transfected with pCMV-HA-PP2A/A $\alpha$ -YFPC and pcDNAI-YFPN-B55 $\alpha$ HA or empty vector were immunoprecipitated (IP) by a pan-anti-B55 antibody or by preimmune IgG as a control, and the immunocomplexes were analyzed by SDS-PAGE and Western blotting by specific anti-PP2A/A $\alpha$ , anti-HA, and anti-PP2A $\alpha$  antibodies. The asterisk indicates

YFPN-B55 $\alpha$ HA. (B–E) Lysates of NIH3T3 cells co-transfected with pCMV-HA-PP2A/A $\alpha$ -YFPC and pcDNAI-YFPN-FLAG-B55 $\beta$ 1, pcDNAI-YFPN-FLAG-B55 $\beta$ 2, pcDNAI-YFPN-FLAG-B55 $\delta$ , pcDNAI-YFPN-FLAG-B55 $\beta\alpha\beta$ , or empty vector were immunoprecipitated (IP) by anti-FLAG-Sepharose, and the immunocomplexes were analyzed by SDS-PAGE and Western blotting (WB) by specific anti-PP2A/A $\alpha$ , anti-FLAG, and anti-PP2A $\alpha$  antibodies. (F) Lysates of NIH3T3 cells co-transfected with pcDNAI-YFPC-PP2A/A $\alpha$  and pcDNAI-YFPN-B56 $\gamma$ 3HA or empty vector were immunoprecipitated (IP) by anti-HA antibody, and the immunocomplexes were analyzed by SDS-PAGE and Western blotting by specific anti-PP2A/A $\alpha$ , anti-HA, and anti-PP2A $\alpha$  antibodies.

[doi:10.1371/journal.pone.0116074.s005](https://doi.org/10.1371/journal.pone.0116074.s005) (PDF)

**S6 Fig. BiFC analysis of various combinations of paired BiFC expression constructs encoding YN- or YC-fused PP2A $\alpha$  and YC- or YN-fused B55 $\beta$ 1 with or without co-expression of 6myc-PP2A/A $\alpha$ .** Equal amounts of BiFC expression constructs encoding YN- or YC-fused PP2A $\alpha$  and YC- or YN-fused B55 $\beta$ 1 with or without equal amounts of pCA2-6myc-PP2A/A $\alpha$  or vector were co-transfected into NIH3T3 cells, and 24 h after transfection, YFP signals due to BiFC were measured by direct fluorescence microscopy and expression of 6myc-PP2A/A $\alpha$  was confirmed by indirect immunofluorescence using anti-Myc tag antibody in conjunction with Cy3-conjugated secondary antibody. DAPI was applied for staining of nuclei. Scale bar: 50  $\mu$ m.

[doi:10.1371/journal.pone.0116074.s006](https://doi.org/10.1371/journal.pone.0116074.s006) (PDF)

**S7 Fig. BiFC analysis of various combinations of paired BiFC expression constructs encoding YN- or YC-fused PP2A $\alpha$  and YC- or YN-fused B56 $\gamma$ 3 with or without co-expression of 6myc-PP2A/A $\alpha$ .** Equal amounts of BiFC expression constructs encoding YN- or YC-fused PP2A $\alpha$  and YC- or YN-fused B56 $\gamma$ 3 with or without equal amounts of pCA2-6myc-PP2A/A $\alpha$  or vector were co-transfected into NIH3T3 cells, and 24 h after transfection, YFP signals due to BiFC were measured by direct fluorescence microscopy and expression of 6myc-PP2A/A $\alpha$  was confirmed by indirect immunofluorescence using anti-Myc tag antibody in conjunction with Cy3-conjugated secondary antibody. DAPI was applied for staining of nuclei. Scale bar: 50  $\mu$ m.

[doi:10.1371/journal.pone.0116074.s007](https://doi.org/10.1371/journal.pone.0116074.s007) (PDF)

**S8 Fig. BiFC analysis of various combinations of paired BiFC expression constructs encoding YN- or YC-fused PP2A $\alpha$  and YC- or YN-fused B55 $\delta$  with or without co-expression of 6myc-PP2A/A $\alpha$ .** Equal amounts of BiFC expression constructs encoding YN- or YC-fused PP2A $\alpha$  and YC- or YN-fused B55 $\delta$  with or without equal amounts of pCA2-6myc-PP2A/A $\alpha$  or vector were co-transfected into NIH3T3 cells, and 24 h after transfection, YFP signals due to BiFC were measured by direct fluorescence microscopy and expression of 6myc-PP2A/A $\alpha$  was confirmed by indirect immunofluorescence using anti-Myc tag antibody in conjunction with Cy3-conjugated secondary antibody. DAPI was applied for staining of nuclei. Scale bar: 50  $\mu$ m.

[doi:10.1371/journal.pone.0116074.s008](https://doi.org/10.1371/journal.pone.0116074.s008) (PDF)

**S9 Fig. Co-immunoprecipitation of BiFC complexes of PP2A $\alpha$ -YC and YN-B55 $\beta$ 1 or YN-B55 $\delta$  in the presence of 6myc-PP2A/A $\alpha$ .** Lysates of NIH3T3 cells co-transfected with equal amounts of BiFC expression constructs encoding PP2A $\alpha$ -YC and YN-B55 $\beta$ 1 or YN-B55 $\delta$  with or without pCA2-6myc-PP2A/A $\alpha$  were immunoprecipitated by anti-HA antibody and the immunocomplexes were analyzed by SDS-PAGE and Western blotting by specific anti-GFP, anti-HA, and anti-Myc tag antibodies.

[doi:10.1371/journal.pone.0116074.s009](https://doi.org/10.1371/journal.pone.0116074.s009) (PDF)

**S10 Fig. BiFC between A $\alpha$ -YC and YN-B55 $\alpha$ , YN-fused B55 $\beta$ 1, B55 $\beta$ 2, B55 $\beta\alpha\beta$ , or B55 $\delta$  and BiFC between YC-A $\alpha$  and YN-B56 $\gamma$ 3 is disrupted by SV40 SMT.** BiFC expression constructs encoding A $\alpha$ -YC and YN-fused B55 $\alpha$ , B55 $\beta$ 1, B55 $\beta$ 2, B55 $\beta\alpha\beta$ , or B55 $\delta$  and BiFC expression constructs encoding YC-A $\alpha$  and YN-B56 $\gamma$ 3 with pCMV5 SMT<sub>WT</sub>, -SMT<sub>MUT</sub>, or empty vector with a 1:1:2 ratio (A $\alpha$ -YC or YC-A $\alpha$ :YN-B:pCMV5-SMT<sub>WT</sub>, pCMV5-SMT<sub>MUT</sub>, or empty vector = 1:1:2), were transfected into NIH3T3 cells, and 24 h after transfection, YFP signals due to BiFC were measured by fluorescence microscopy. Expression of HA-tagged YN-fused B55 $\alpha$ , B55 $\beta$ 1, B55 $\beta$ 2, B55 $\beta\alpha\beta$ , B55 $\delta$ , or B56 $\gamma$ 3 was confirmed using anti-HA antibody by indirect immunofluorescence microscopy as described earlier. DAPI was applied for staining of nuclei. Scale bar: 50  $\mu$ m.

[doi:10.1371/journal.pone.0116074.s010](https://doi.org/10.1371/journal.pone.0116074.s010) (PDF)

**S1 Table. Plasmids used in this study.**

[doi:10.1371/journal.pone.0116074.s011](https://doi.org/10.1371/journal.pone.0116074.s011) (PDF)

**S2 Table. Primers used in this study.**

[doi:10.1371/journal.pone.0116074.s012](https://doi.org/10.1371/journal.pone.0116074.s012) (PDF)

**S1 Text. Construction of expression plasmids.**

[doi:10.1371/journal.pone.0116074.s013](https://doi.org/10.1371/journal.pone.0116074.s013) (PDF)

## Acknowledgments

We are grateful to Drs. Catherine Berlot and Tom Kerppola for providing the BiFC expression vectors, Dr. David Virshup for providing the mammalian expression vector for B subunits, Dr. Estelle Sontag for the SV40 SMTwt and SMTmut expression vectors, and Dr. Stefan Strack for the B55 $\beta$ 2wt and B55 $\beta$ 2mut expression vectors. We are thankful to Drs. Brian K. Law and Sherry S. Wang for valuable comments on the manuscript.

## Author Contributions

Conceived and designed the experiments: CWC BEW. Performed the experiments: STM SJC YLC TYL CEC. Analyzed the data: STM SJC YLC TYL SCHK. Contributed reagents/materials/analysis tools: YCC KMR NSC. Wrote the paper: CWC BEW.

## References

1. **Janssens V, Goris J** (2001) Protein phosphatase 2A: a highly regulated family of serine/threonine phosphatases implicated in cell growth and signalling. *Biochem J* 353: 417–439.
2. **Healy AM, Zolnierowicz S, Stapleton AE, Goebel M, DePaoli-Roach AA, et al.** (1991) CDC55, a *Saccharomyces cerevisiae* gene involved in cellular morphogenesis: identification, characterization, and homology to the B subunit of mammalian type 2A protein phosphatase. *Mol Cell Biol* 11: 5767–5780.
3. **Mayer RE, Hendrix P, Cron P, Matthies R, Stone SR, et al.** (1991) Structure of the 55-kDa regulatory subunit of protein phosphatase 2A: evidence for a neuronal-specific isoform. *Biochemistry* 30: 3589–3597.
4. **Zolnierowicz S, Csontos C, Bondor J, Verin A, Mumby MC, et al.** (1994) Diversity in the regulatory B-subunits of protein phosphatase 2A: identification of a novel isoform highly expressed in brain. *Biochemistry* 33: 11858–11867.
5. **McCright B, Virshup DM** (1995) Identification of a new family of protein phosphatase 2A regulatory subunits. *J Biol Chem* 270: 26123–26128.
6. **Csontos C, Zolnierowicz S, Bako E, Durbin SD, DePaoli-Roach AA** (1996) High complexity in the expression of the B' subunit of protein phosphatase 2A0. Evidence for the existence of at least seven novel isoforms. *J Biol Chem* 271: 2578–2588.
7. **Hendrix P, Mayer-Jackel RE, Cron P, Goris J, Hofsteenge J, et al.** (1993) Structure and expression of a 72-kDa regulatory subunit of protein phosphatase 2A. Evidence for different size forms produced by alternative splicing. *J Biol Chem* 268: 15267–15276.
8. **Moreno CS, Park S, Nelson K, Ashby D, Hubalek F, et al.** (2000) WD40 repeat proteins striatin and S/G(2) nuclear autoantigen are members of a novel family of calmodulin-binding proteins that associate with protein phosphatase 2A. *J Biol Chem* 275: 5257–5263.
9. **Dagda RK, Zaucha JA, Wadzinski BE, Strack S** (2003) A developmentally regulated, neuron-specific splice variant of the variable subunit Bbeta targets protein phosphatase 2A to mitochondria and modulates apoptosis. *J Biol Chem* 278: 24976–24985.
10. **Strack S, Zaucha JA, Ebner FF, Colbran RJ, Wadzinski BE** (1998) Brain protein phosphatase 2A: developmental regulation and distinct cellular and subcellular localization by B subunits. *J Comp Neurol* 392: 515–527.
11. **McCright B, Rivers AM, Audlin S, Virshup DM** (1996) The B56 family of protein phosphatase 2A (PP2A) regulatory subunits encodes differentiation-induced phosphoproteins that target PP2A to both nucleus and cytoplasm. *J Biol Chem* 271: 22081–22089.
12. **Gentry MS, Hallberg RL** (2002) Localization of *Saccharomyces cerevisiae* protein phosphatase 2A subunits throughout mitotic cell cycle. *Mol Biol Cell* 13: 3477–3492.
13. **Di Como CJ, Arndt KT** (1996) Nutrients, via the Tor proteins, stimulate the association of Tap42 with type 2A phosphatases. *Genes Dev* 10: 1904–1916.
14. **Murata K, Wu J, Brautigan DL** (1997) B cell receptor-associated protein alpha4 displays rapamycin-sensitive binding directly to the catalytic subunit of protein phosphatase 2A. *Proc Natl Acad Sci U S A* 94: 10624–10629.
15. **Inui S, Sanjo H, Maeda K, Yamamoto H, Miyamoto E, et al.** (1998) Ig receptor binding protein 1 (alpha4) is associated with a rapamycin-sensitive signal transduction in lymphocytes through direct binding to the catalytic subunit of protein phosphatase 2A. *Blood* 92: 539–546.
16. **Kong M, Fox CJ, Mu J, Solt L, Xu A, et al.** (2004) The PP2A-associated protein alpha4 is an essential inhibitor of apoptosis. *Science* 306: 695–698.
17. **Kong M, Ditsworth D, Lindsten T, Thompson CB** (2009) Alpha4 is an essential regulator of PP2A phosphatase activity. *Mol Cell* 36: 51–60.
18. **Kong M, Bui TV, Ditsworth D, Gruber JJ, Goncharov D, et al.** (2007) The PP2A-associated protein alpha4 plays a critical role in the regulation of cell spreading and migration. *J Biol Chem* 282: 29712–29720.
19. **Watkins GR, Wang N, Mazalouskas MD, Gomez RJ, Guthrie CR, et al.** (2012) Monoubiquitination promotes calpain cleavage of the protein phosphatase 2A (PP2A) regulatory subunit alpha4, altering PP2A stability and microtubule-associated protein phosphorylation. *J Biol Chem* 287: 24207–24215.

20. **Wang N, Leung HT, Mazalouskas MD, Watkins GR, Gomez RJ, et al.** (2012) Essential roles of the Tap42-regulated protein phosphatase 2A (PP2A) family in wing imaginal disc development of *Drosophila melanogaster*. *PLoS One* 7: e38569.
21. **Jiang L, Stanevich V, Satyshur KA, Kong M, Watkins GR, et al.** (2013) Structural basis of protein phosphatase 2A stable latency. *Nat Commun* 4: 1699.
22. **Janssens V, Longin S, Goris J** (2008) PP2A holoenzyme assembly: in cauda venenum (the sting is in the tail). *Trends Biochem Sci* 33: 113–121.
23. **Kerppola TK** (2008) Bimolecular fluorescence complementation: visualization of molecular interactions in living cells. *Methods Cell Biol* 85: 431–470.
24. **Forster T** (1959) 10th Spiers Memorial Lecture. Transfer mechanisms of electronic excitation. *Discuss Faraday Soc* 27: 7–17.
25. **Jares-Erijman EA, Jovin TM** (2003) FRET imaging. *Nat Biotechnol* 21: 1387–1395.
26. **Shi Y** (2009) Serine/threonine phosphatases: mechanism through structure. *Cell* 139: 468–484.
27. **Shyu YJ, Suarez CD, Hu CD** (2008) Visualization of AP-1 NF-kappaB ternary complexes in living cells by using a BiFC-based FRET. *Proc Natl Acad Sci U S A* 105: 151–156.
28. **Kuo YC, Huang KY, Yang CH, Yang YS, Lee WY, et al.** (2008) Regulation of phosphorylation of Thr-308 of Akt, cell proliferation, and survival by the B55alpha regulatory subunit targeting of the protein phosphatase 2A holoenzyme to Akt. *J Biol Chem* 283: 1882–1892.
29. **Lee TY, Lai TY, Lin SC, Wu CW, Ni IF, et al.** (2010) The B56gamma3 regulatory subunit of protein phosphatase 2A (PP2A) regulates S phase-specific nuclear accumulation of PP2A and the G1 to S transition. *J Biol Chem* 285: 21567–21580.
30. **Youvan DC, Silva CM, Bylina EJ, Coleman WJ, Dilworth MR, et al.** (1997) Calibration of Fluorescence Resonance Energy Transfer in Microscopy Using Genetically Engineered GFP Derivatives on Nickel Chelating Beads. *Biotechnol et alia* 3: 1–18.
31. **Strack S, Chang D, Zaucha JA, Colbran RJ, Wadzinski BE** (1999) Cloning and characterization of B delta, a novel regulatory subunit of protein phosphatase 2A. *FEBS Lett* 460: 462–466.
32. **Strack S, Kini S, Ebner FF, Wadzinski BE, Colbran RJ** (1999) Differential cellular and subcellular localization of protein phosphatase 1 isoforms in brain. *J Comp Neurol* 413: 373–384.
33. **Mumby M** (1995) Regulation by tumour antigens defines a role for PP2A in signal transduction. *Semin Cancer Biol* 6: 229–237.
34. **Sontag E, Fedorov S, Kamibayashi C, Robbins D, Cobb M, et al.** (1993) The interaction of SV40 small tumor antigen with protein phosphatase 2A stimulates the map kinase pathway and induces cell proliferation. *Cell* 75: 887–897.
35. **Yang J, Roe SM, Prickett TD, Brautigam DL, Barford D** (2007) The structure of Tap42/alpha4 reveals a tetratricopeptide repeat-like fold and provides insights into PP2A regulation. *Biochemistry* 46: 8807–8815.
36. **McConnell JL, Watkins GR, Soss SE, Franz HS, McCorvey LR, et al.** (2010) Alpha4 is a ubiquitin-binding protein that regulates protein serine/threonine phosphatase 2A ubiquitination. *Biochemistry* 49: 1713–1718.
37. **Tung HY, Alemany S, Cohen P** (1985) The protein phosphatases involved in cellular regulation. 2. Purification, subunit structure and properties of protein phosphatases-2A0, 2A1, and 2A2 from rabbit skeletal muscle. *Eur J Biochem* 148: 253–263.
38. **Kremmer E, Ohst K, Kiefer J, Brewis N, Walter G** (1997) Separation of PP2A core enzyme and holoenzyme with monoclonal antibodies against the regulatory A subunit: abundant expression of both forms in cells. *Mol Cell Biol* 17: 1692–1701.
39. **Xu Y, Xing Y, Chen Y, Chao Y, Lin Z, et al.** (2006) Structure of the protein phosphatase 2A holoenzyme. *Cell* 127: 1239–1251.
40. **Cho US, Xu W** (2007) Crystal structure of a protein phosphatase 2A heterotrimeric holoenzyme. *Nature* 445: 53–57.

41. **Wadzinski BE, Eisfelder BJ, Peruski LF Jr, Mumby MC, Johnson GL** (1992) NH<sub>2</sub>-terminal modification of the phosphatase 2A catalytic subunit allows functional expression in mammalian cells. *J Biol Chem* 267: 16883–16888.
42. **Baharians Z, Schonthal AH** (1998) Autoregulation of protein phosphatase type 2A expression. *J Biol Chem* 273: 19019–19024.
43. **Chung H, Nairn AC, Murata K, Brautigan DL** (1999) Mutation of Tyr307 and Leu309 in the protein phosphatase 2A catalytic subunit favors association with the alpha 4 subunit which promotes dephosphorylation of elongation factor-2. *Biochemistry* 38: 10371–10376.
44. **Xu Y, Chen Y, Zhang P, Jeffrey PD, Shi Y** (2008) Structure of a protein phosphatase 2A holoenzyme: insights into B55-mediated Tau dephosphorylation. *Mol Cell* 31: 873–885.
45. **Giepmans BN, Adams SR, Ellisman MH, Tsien RY** (2006) The fluorescent toolbox for assessing protein location and function. *Science* 312: 217–224.
46. **Ito A, Koma Y, Sohda M, Watabe K, Nagano T, et al.** (2003) Localization of the PP2A B56gamma regulatory subunit at the Golgi complex: possible role in vesicle transport and migration. *Am J Pathol* 162: 479–489.
47. **Pallas DC, Shahrik LK, Martin BL, Jaspers S, Miller TB, et al.** (1990) Polyoma small and middle T antigens and SV40 small t antigen form stable complexes with protein phosphatase 2A. *Cell* 60: 167–176.
48. **Harper JV** (2005) Synchronization of cell populations in G<sub>1</sub>/S and G<sub>2</sub>/M phases of the cell cycle. *Methods Mol Biol* 296: 157–166.